

Phonon-Enhanced Near-Field Spectroscopy to Extract the Local Electronic Properties of Buried 2D Electron Systems in Oxide Heterostructures

Julian Barnett, Marc-André Rose, Georg Ulrich, Martin Lewin, Bernd Kästner, Arne Hoehl, Regina Dittmann, Felix Gunkel, and Thomas Taubner*

In the family of functional oxide materials, the interface between LaAlO_3 and SrTiO_3 (LAO/STO) is an interesting example, as both materials are large-bandgap insulators in their bulk state but give rise to a confined 2D electron gas (2DEG) when combined through thin-film deposition. While this 2DEG exhibits remarkable properties, its experimental investigation is mostly limited to destructive or non-local (i.e. averaging over larger areas) methods until recently. Scanning near-field optical microscopy is shown to overcome this limitation, detecting buried 2DEGs by using highly confined optical near-fields. Here, a full spectroscopic approach with phonon-enhancement and simulations based on the finite dipole model is combined to extract quantitative electronic properties of the interfacial LAO/STO 2DEG. This three-fold improvement compared to previous work will enable the quantitative nanoscale, non-destructive, sub-surface analysis of complex oxide thin films and interfaces, as well as similar heterostructures.

transitions.^[1] Their properties can be finely tuned by controlling the material deposition and post-deposition parameters, as their electronic behavior is strongly dependent on the local defect structure and lattice.^[2,3] Symmetry breaking at interfaces even gives rise to phenomena which neither bulk material possesses, such as magnetic ordering at the interface of non-magnetic materials^[4,5,6] or charge-transfer at a variety of oxide heterointerfaces, leading to highly confined 2D electron systems between two bulk insulators.^[7,8] Because of their complex correlated nature, investigating these effects requires probing of subsurface properties in a non-destructive manner.


The heterointerface of LaAlO_3 (LAO) and SrTiO_3 (STO) is a popular example of charge-transfer, exhibiting a 2D electron gas (2DEG) with surprising properties^[6–9] when at least 4 unit cells (uc) of LAO are deposited on an STO substrate with TiO_2 termination. The strong dependence of the electrons on the local ionic structure offers a large amount of influence on the material properties via defect and interface engineering.^[10,11] Modern thin-film deposition technology is sufficiently advanced to grow epitaxial interfaces with unit cell precision.^[12] Nevertheless, it is imperative to improve our understanding of the complex interplay of factors in the charge-transfer mechanism in complex oxide heterostructures. Therefore, the local electronic properties need to be investigated quantitatively. This requires an analytical technology with three key properties: sensitivity to charge carriers, nanoscale resolution, and subsurface sensitivity even below insulating layers.

Scattering-type near-field optical microscopy (s-SNOM) is a technique which fulfils these criteria, as it uses strongly confined near-fields penetrating the sample, locally probing its dielectric function with subwavelength resolution.^[13] Previous s-SNOM investigations of the LAO/STO interface were able to demonstrate the ability of the technique to detect the presence of 2DEG electrons^[14] and even extract rudimentary information about the electronic properties from near-field optical properties.^[15] While this enables the detection of inhomogeneities in principle, a more detailed spectroscopic understanding of local electronic properties, such as charge carrier density and mobility, is necessary to evaluate the impact of different types of defects and enable precise and reproducible fabrication of devices.

1. Introduction

Complex transition metal oxides and their heterostructures offer a large variety of interesting phenomena, such as superconductivity, multiferroics, and metal-insulator

J. Barnett, Dr. M. Lewin, Prof. T. Taubner
 I. Institute of Physics (IA)
 RWTH Aachen
 Sommerfeldstr. 14, Aachen 52074, Germany
 E-mail: taubner@physik.rwth-aachen.de
 M.-A. Rose, Dr. F. Gunkel
 Institut für Werkstoffe der Elektrotechnik (IWE2)
 RWTH Aachen
 Sommerfeldstr. 18, Aachen 52074, Germany
 G. Ulrich, Dr. B. Kästner, A. Hoehl
 Physikalisch-Technische Bundesanstalt
 Magnusstr. 9, Berlin 12489, Germany
 Prof. R. Dittmann, Dr. F. Gunkel
 Peter Grünberg Institute
 Forschungszentrum Jülich
 Wilhelm-Johnen-Str., Jülich 52428, Germany

 The ORCID identification number(s) for the author(s) of this article can be found under <https://doi.org/10.1002/adfm.202004767>.

© 2020 The Authors. Published by Wiley-VCH GmbH. This is an open access article under the terms of the Creative Commons Attribution License, which permits use, distribution and reproduction in any medium, provided the original work is properly cited.

DOI: 10.1002/adfm.202004767

In this work, we show for the first time that the combination of phonon-enhanced near-field spectroscopy with broadband nanoscale Fourier-transform Infrared Spectroscopy (nano-FTIR) and careful modeling can yield additional information about the local electronic properties of the 2DEG at the LAO/STO interface. We demonstrate termination-sensitivity and decouple interface contributions in the near-field signal from thin film and substrate contributions, in order to systematically extract the dielectric properties of the 2DEG. To achieve this, we use broadband synchrotron radiation from a storage ring with s-SNOM in a nano-FTIR setup^[16] and compare these measurements to theoretical simulations using a combination of the Finite Dipole Model (FDM) and Transfer Matrix Method.^[17] Our approach can be universally applied to the non-destructive optical analysis of buried electron systems.

1.1. Complex Oxides and the LAO/STO Interface

In complex oxides, strong electron correlations lead to entanglement of charge, spin, and orbital degrees of freedom at a given lattice site,^[6] which in turn give rise to the aforementioned fundamentally intertwined interface phenomena. The prospect for devices with tailor-made properties is certainly exciting;^[18] however, the high sensitivity of electrons to their local environment can also be challenging. Examples are the abrupt change in properties around the critical thickness of the LAO layer as well as the influence of defects on the 2DEG number of charge carriers and their mobility.^[10,19,20] Additionally, the electronic reconstruction in LAO/STO is dependent on the topmost layer (termination) of the STO substrate (Figure 1a), as it determines the polarity in the LAO layer: while a 2DEG will form on a TiO₂-terminated substrate, for a SrO-terminated substrate the interface usually remains non-conductive, as the diverging potential can be compensated by oxygen vacancies.^[7,21] Taking all effects together, mixed termination of the substrate, LAO thicknesses varying around the critical value of 4 uc, and the presence of additional defects should strongly influence the homogeneity of 2DEG formation. The deconvolution of the intricate interplay

of these effects is a much-discussed topic in the scientific field. Therefore, the impact of fabrication parameters on the local electronic properties have to be monitored carefully and evaluated quantitatively, which is possible with near-field spectroscopy.

1.2. Near-Field Spectroscopy of the LAO/STO Interface

Scattering-type near-field optical microscopy (s-SNOM) is a technique that locally probes the dielectric function with a lateral resolution independent of the incidental wavelength of light and far below the diffraction limit.^[22] This is achieved by focusing light on a metallic tip (Figure 1b), resulting in strong electromagnetic near-fields at the apex that polarize the sample within a confined volume and re-radiate scattered fields, which contain information about the coupled tip-sample system. By modulating the distance between tip and sample with a frequency Ω_{tip} , higher-order demodulation of the scattered signal at $n\Omega_{\text{tip}}$ allows for separation of the strongly nonlinear near-field and the background. Additionally, an interferometric setup enables separate detection of amplitude s_n and phase ϕ_n at the detector. 2D optical images of the sample can be acquired by using narrow-band laser illumination while scanning the surface, resulting in optical contrast based on local variations in the dielectric function of the material at a certain wavelength.^[23] Alternatively, by employing broad-band illumination and a moveable reference mirror in a Michelson-type interferometric setup, nano-FTIR can yield information about local optical properties in a broad spectral range.^[24]

First published s-SNOM images on the LAO/STO system were indeed able to show significant optical contrast between regions with and without 2DEG.^[14] While this proves that the method is sensitive to the presence of free charge carriers buried below the insulating LAO top layer, the results were purely qualitative and did not yield any conclusions on electronic properties, such as charge carrier density, mobility, or effective mass. More recently,^[15] Luo et al. were able to investigate a similar sample at three discrete wavelengths and a range of temperatures between 6 and 300 K, impressively demonstrating

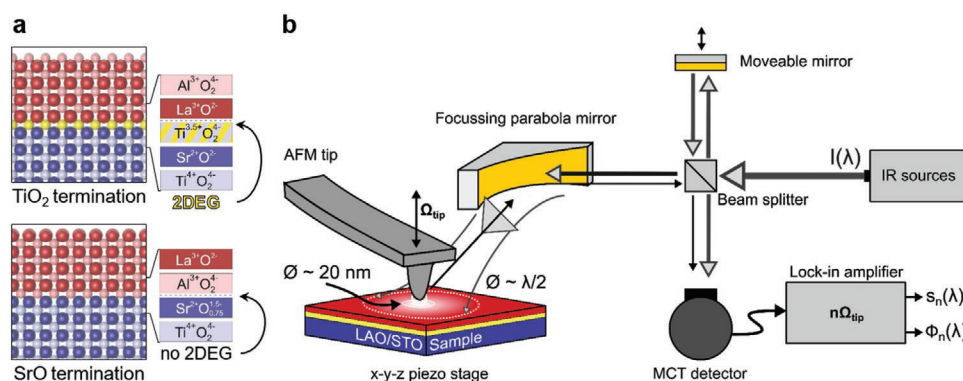


Figure 1. Termination-dependence and experimental setup. a) Formation of the 2DEG depends on the topmost layer (termination) of the STO substrate. b) Schematic of the experimental setup showing the optical beam path from light sources (laser or broadband synchrotron radiation from the electron storage ring MLS) to detector, with interferometric setup and AFM cantilever in between; the parabolic mirror focuses light to a diffraction-limited spot, while the detected near-fields result from a much smaller spot size linked to the tip radius. Background suppression is achieved by using a lock-in amplifier at $n\Omega_{\text{tip}}$ (higher harmonic frequencies of the tip oscillation, with $n = 2$) and the interferometric setup enables separation of the detected signals into amplitude s_n and phase ϕ_n .

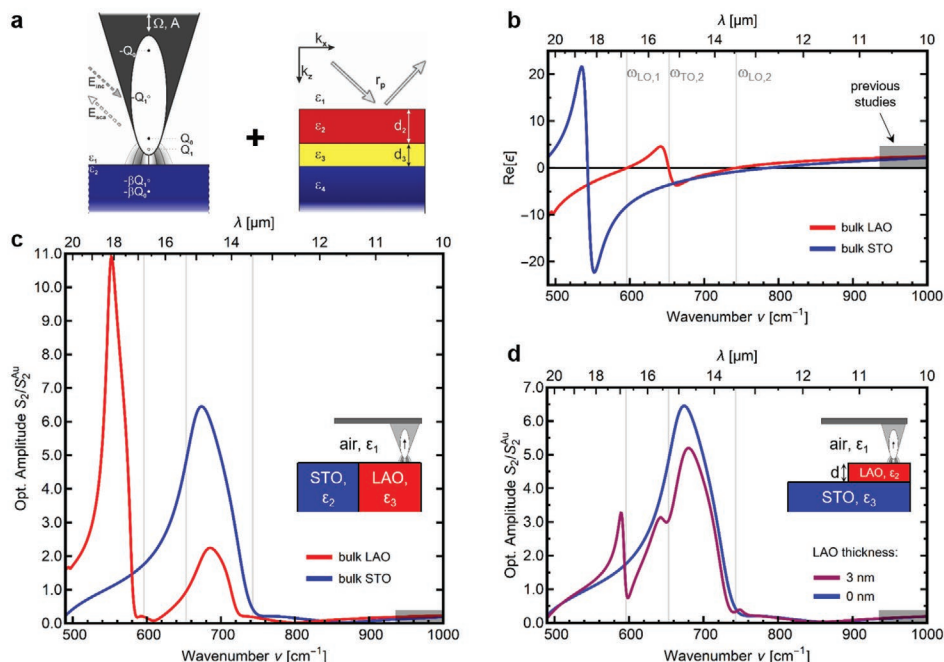


Figure 2. Modelling of near-field contrasts. a) Schematic depiction of the finite dipole model (FDM, left) and transfer matrix method (right), used in s-SNOM contrast simulations^[17] (see Experimental Section and Supporting Information for details). b) Bulk dielectric functions of STO and LAO (real part) as modelled^[30] using literature values;^[31,32] vertical grey lines indicate zero-crossings (TO- and LO-frequencies) of $\text{Re}[\epsilon_{\text{LAO}}]$ for comparison. c) Calculated near-field contrast spectra (cf. Supporting Information) of bulk STO (blue) and bulk LAO (red), respectively. d) Calculated near-field contrast spectra of the layered system (LAO thickness of 8 unit cells) without 2DEG, that is, only taking phonon modes of the two materials into account. The shadowed rectangles in (b–d) illustrate the spectral range of previous studies.

the capabilities of cryo-SNOM,^[25] but only presenting minimal spectroscopic insight into electronic properties.

Due to strong coupling between the near-fields of tip and sample, a resonance occurs for negative values of the sample dielectric function,^[26] that is, between transversal optical (TO) frequency ω_{TO} and longitudinal optical (LO) frequency ω_{LO} in the case of phonon resonances (cf. **Figure 2**) or below the plasma frequency ω_p in the case of free charge carriers. While significantly enhancing the scattering amplitude, the strong coupling between tip and sample complicates the direct extraction of sample properties from s-SNOM spectroscopy.^[27] In these circumstances, careful electromagnetic modeling with known dielectric functions is the preferred approach. Using a simple point dipole model for layered structures, Luo et al. were able to convincingly argue that temperature-dependent changes in s-SNOM contrast could be attributed to a change in electron mobility, successfully opening the door for quantitative analysis of subsurface electronic properties. So far, all previous s-SNOM publications on LAO/STO have focused on a frequency range accessible with a CO₂ laser (935–1075 cm⁻¹, i.e., 10.7–9.3 μm, shadowed rectangles in Figures 2–4), which is outside the phonon resonances of both STO and LAO.

Unfortunately, in this spectral region the s-SNOM contrast is comparatively low and frequency-independent, reducing the added value of varying the illumination wavelength and resulting in ambiguity when comparing experimental results to simulations. In direct contrast, it was shown that the presence of free charge carriers leads to significant and characteristic changes to the phonon resonance in doped STO ceramics due

to plasmon–phonon coupling.^[3] Exploiting this relationship enables the quantitative extraction of electronic properties from measurements in the phonon spectral region. Following this approach, our work focuses on broadband nano-FTIR investigations of LAO/STO phonons, obtaining continuous spectra with multiple characteristic features and thereby dramatically increasing the amount of information available for fitting to theoretical predictions. This allows us to systematically deconvolute thin film, bulk, and interface contributions. Additionally, compared to the Point Dipole Model used in the previous work, our simulations of layered systems are based on an improved model that takes into account the elongated shape of the probing tip (Finite Dipole Model, cf. Figure 2a) and yields more accurate predictions of spectroscopic s-SNOM contrast in the range of material resonances.^[28] We thereby make the analysis of phonon resonances useful for nanoscale layered oxide heterostructures with buried electron systems and—beyond that—for any heterostructure where phonons and electrons concur.

2. Results and Discussion

2.1. Influence of the LAO Thickness on the Near-Field Response

As previously stated, modelling the near-field contrast is an essential step of data analysis because s-SNOM scattering signals depend on the local dielectric function in a non-trivial way due to resonant tip-sample coupling (see Supporting Information for details). Hence, it is necessary to incorporate

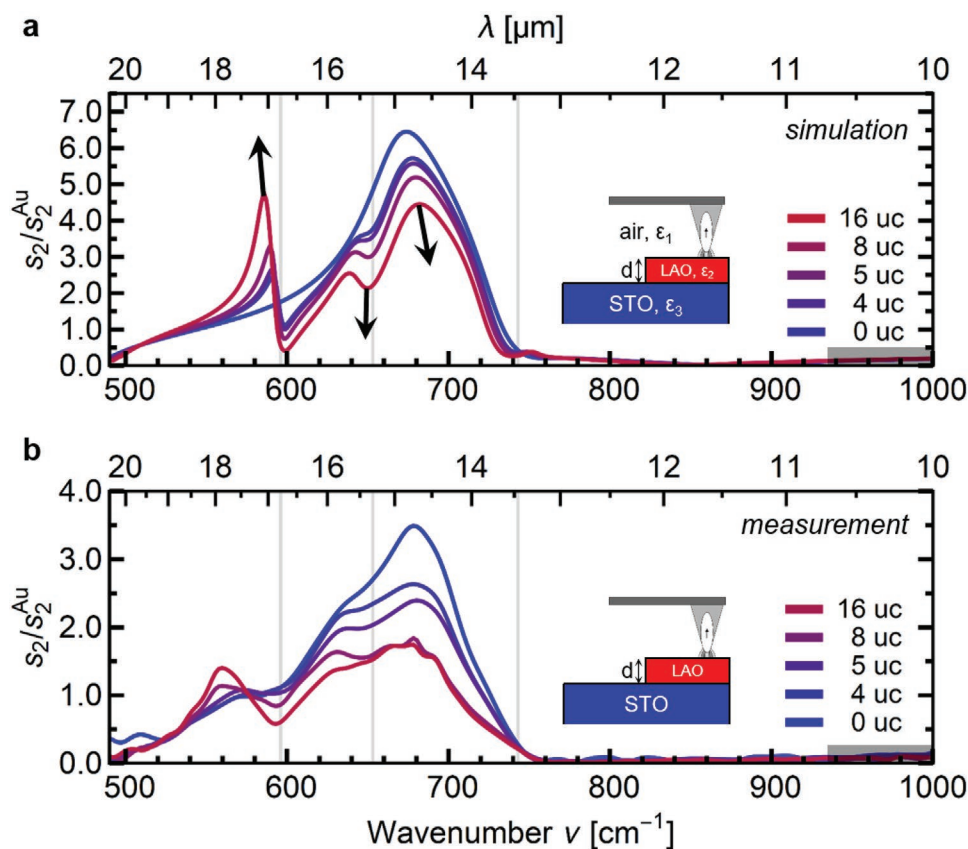


Figure 3. Comparison of simulation and measurement of Au-normalized scattering amplitude of demodulation order $n = 2$. a) Simulation of near-field contrast spectra of the layered system (similar to Figure 2d) neglecting 2DEG, that is, only taking into account the phonon resonances of both materials. Vertical grey lines are indicating the zero crossings of $\text{Re}[\epsilon_{\text{LAO}}]$ for comparison. b) Measurements of LAO/STO samples with the respective LAO thickness d in unit cells (uc). All samples are above the critical threshold of 4 uc and feature a 2DEG. The shadowed rectangles in (a, b) illustrate spectral overlap with previous publications.

prior knowledge about the sample into theoretical considerations, such as an estimate of the local dielectric function and the number and thickness of layers (cf. Figure 2a), to ensure a valid starting point for any fitting procedures. Additionally, even ultra-thin surface layers with a thickness below 5 nm can significantly influence the s-SNOM contrast beyond mere dielectric screening if they exhibit resonant behavior in the spectral region of interest. This exceptional surface sensitivity was previously shown for phonon resonances of the native oxide on doped silicon nanowires,^[29] and therefore has to be implemented for a quantitative analysis.

To investigate the relevance of this surface layer effect for LAO/STO samples, Figure 2b shows the real part of the dielectric functions $\text{Re}[\epsilon]$ of LAO (red) and STO (blue) in the spectral region between 500 and 1000 cm^{-1} , following the Lorentz oscillator model. Due to the strong nature of the oscillators, $\text{Re}[\epsilon]$ reaches negative values between ω_{TO} and ω_{LO} , for example, from 540 to 800 cm^{-1} for the STO resonance shown. Figure 2b also indicates that LAO does not behave like a dielectric cover layer in this spectral range, but instead exhibits two phonon resonances, with zero-crossings of $\text{Re}[\epsilon_{\text{LAO}}]$ between the respective TO and LO frequencies indicated by vertical grey lines ($\omega_{\text{TO},1} = 427 \text{ cm}^{-1}$ not shown). As tip-sample coupling and thus s-SNOM contrast is strongest for slightly negative $\text{Re}[\epsilon]$ of

the sample,^[26] it is expected that these additional sign changes of the permittivity at the surface—where the near-fields are highest—will influence the s-SNOM signal significantly. Indeed, comparing the simulated (cf. Experimental Section) s-SNOM response of bulk STO and bulk LAO (Figure 2c), one resonance peak shows up in the scattering signal of bulk STO (blue) at around 675 cm^{-1} , corresponding to a dielectric function of $\text{Re}[\epsilon_{\text{STO}}] \approx -3$, close to the LO frequency of the relevant STO phonon. The s-SNOM response of bulk LAO (red) clearly yields two resonance peaks at 550 cm^{-1} and 685 cm^{-1} , respectively, hence overlapping with the STO phonon resonance. The strong differences in intensity can be linked to the imaginary part of the dielectric function, as higher damping leads to reduced oscillator strength of the coupled system.

Consequently, instead of merely modifying the dielectric environment of the substrate phonon resonance, adding LAO on top of STO introduces additional phonon resonances (Figure 2d), as shown exemplarily for a system with 8 unit cells (uc) LAO deposited on top of STO, corresponding to a thickness of 3 nm. The resulting resonance pattern follows the overall shape of the STO resonance, but shows three additional characteristic features: an asymmetric resonance around 590 cm^{-1} , a pronounced shoulder at 650 cm^{-1} , and a reduction of the STO peak amplitude around 680 cm^{-1} . No free electrons of the 2DEG are accounted for in

this simulation, only bulk phonon modes of the two materials, showing that even in this simple setup a careful and thorough theoretical treatment of the material system is necessary to understand its non-trivial s-SNOM response.

Figure 3a predicts the influence of increasing thickness of the LAO top layer on the s-SNOM scattering amplitude spectrum, showing a strengthening of the three characteristic features (cf. **Figure 2d**), as indicated by the three black arrows. Intuitively, due to the surface sensitivity of s-SNOM, the STO near-field phonon resonance (blue) should gradually transform into the bulk LAO near-field phonon resonances as the LAO thickness is increased (red in **Figure 2c**), which is visualized by a color transition of the curves towards a red hue. Within the simulation conditions used (cf. Supporting Information), the intensity of the peak below 600 cm^{-1} theoretically surpasses the STO main peak at 680 cm^{-1} already at a thickness of 16 uc (6 nm) of LAO. This demonstrates the added value of full spectroscopic investigations to separate the influence of LAO phonons from the influence of 2DEG free charge carriers on the STO near-field phonon resonance within the spectral region of interest.

The validity of these simulations was confirmed by experiments on LAO/STO heterostructures (**Figure 3b**) using s-SNOM in a nano-FTIR setup with synchrotron radiation (cf. Experimental Section), indeed showing the presence of simulated characteristic features and their dependence on LAO thickness. For the presented scattering amplitude s_2 , the background is already sufficiently suppressed for $n = 2$ due to the long mid-IR wavelengths^[33] (for a comparison to other demodulation orders see Supporting Information). Additional scattering phase spectra can be found in the Supporting Information, but do not add further information to our studies.

Keeping in mind that the LAO thickness is varied between 1.5 nm and 6 nm, corresponding to 4 uc and 16 uc, respectively, the remarkable surface sensitivity of s-SNOM is illustrated, as surface layers can be easily identified and characterized spectroscopically even below 5 nm thickness. Describing the experimental spectra qualitatively, all characteristic features (black arrows in **Figure 3a**) appear broadened, of reduced intensity, and slightly shifted as compared to the simulations, indicating additional contributions to the dielectric function in reality. Using the vertical grey lines (zero-crossings of ϵ_{LAO}) for comparison, it is evident that the peak below 600 cm^{-1} is shifted towards lower wavenumbers, as can be expected^[34] for ultra-thin films with pseudomorphic growth and a lattice mismatch of -2% . The twofold difference in absolute peak height between simulation and experiment could be related to the specific choice of FDM geometric parameters,^[35] while the relative height and overall shape are comparable. A slight modulation of the bulk STO peak around 600 and 650 cm^{-1} is visible, which could be an effect of noise or Au normalization. Nonetheless, the influence of the LAO thickness can be identified from the spectra with confidence.

Allowing for slight variations in peak position, which will have to be addressed in future improvements to the model, the main difference between simulation and measurement is strong damping, most prominent for the STO phonon peak at

680 cm^{-1} . This could be an indicator for the presence of free charge carriers at the interface, as additional Drude contributions to the dielectric function were shown to dampen phonon peaks significantly.^[3] It is therefore necessary to include a corresponding treatment of free charge carriers to the previously described theoretical model.

2.2. Influence of Free Charge Carriers (2DEG) on the Near-Field Response

Figure 4a illustrates the influence of an additional layer of free electrons (yellow) at the interface between LAO and STO, represented by a Drude model with 3D electron density n . We have determined 2DEG electron densities and mobilities of our samples in Hall measurements (cf. Supporting Information), but these are averaged over a large area of the sample and do not allow conclusions on the depth profile of the charge carriers. In this work, the depth profile was approximated according to theoretical and experimental results from the literature^[20,36,37] and further simplified by a uniform distribution. The values chosen for the simulation are varied around the 3D electron density that could be expected from homogeneously distributing the measured 2D electron density of $n_{2D} = 4.34 \times 10^{13}\text{ cm}^{-2}$ over a depth $d_2 = 10\text{ nm}$ (cf. Supporting Information). The average electron mobility of the relevant sample was determined to be $\mu = 5.09\text{ cm}^2\text{ (V}\cdot\text{s)}^{-1}$.

Examining the influence of free electrons on the phonon resonance, as simulated in **Figure 4a**, additional damping on the main peak at 680 cm^{-1} is clearly evident, while the characteristic asymmetric feature of the thin LAO layer around 590 cm^{-1} remains mostly unchanged. The fact that the STO response is influenced more heavily than the LAO response is due to the electronic screening of the underlying STO phonons from tip near-fields. In contrast, the layer on top is barely influenced, as no energy exchange between LAO phonons and 2DEG electrons (e.g., frequency-dependent damping function^[38]) is implemented in the model. Nevertheless, the presence of electrons in the sample explains a major part of the deviations between **Figure 3a,b**, where experimental results indicated stronger damping of the main STO peak than expected from phonon modeling alone. This claim can be verified by experimentally comparing two samples with and without 2DEG, respectively, without changing the properties of the phonon resonances. To achieve the latter, LAO layer thickness and crystallinity have to remain the same, excluding samples below the 4 uc threshold or the utilization of amorphous STO substrates. Instead, fabricating samples with different substrate termination is an elegant solution, as LAO grown on SrO-terminated STO will not lead to the formation of a conducting interface (cf. **Figure 1a**) while the phonon properties remain unchanged. The absence of free carriers in the SrO-terminated sample is evident from X-ray photoemission spectroscopy indicating a pure Ti^{4+} valence state at the interface (cf. Supporting Information).

Figure 4b compares measurements of samples with 8 uc LAO grown on TiO_2 -terminated STO to those with 8 uc LAO grown on SrO-terminated STO. Here, the solid violet curve denotes the sample without electrons at the interface (SrO termination) and within the region of $600\text{--}750\text{ cm}^{-1}$ its normalized scattering

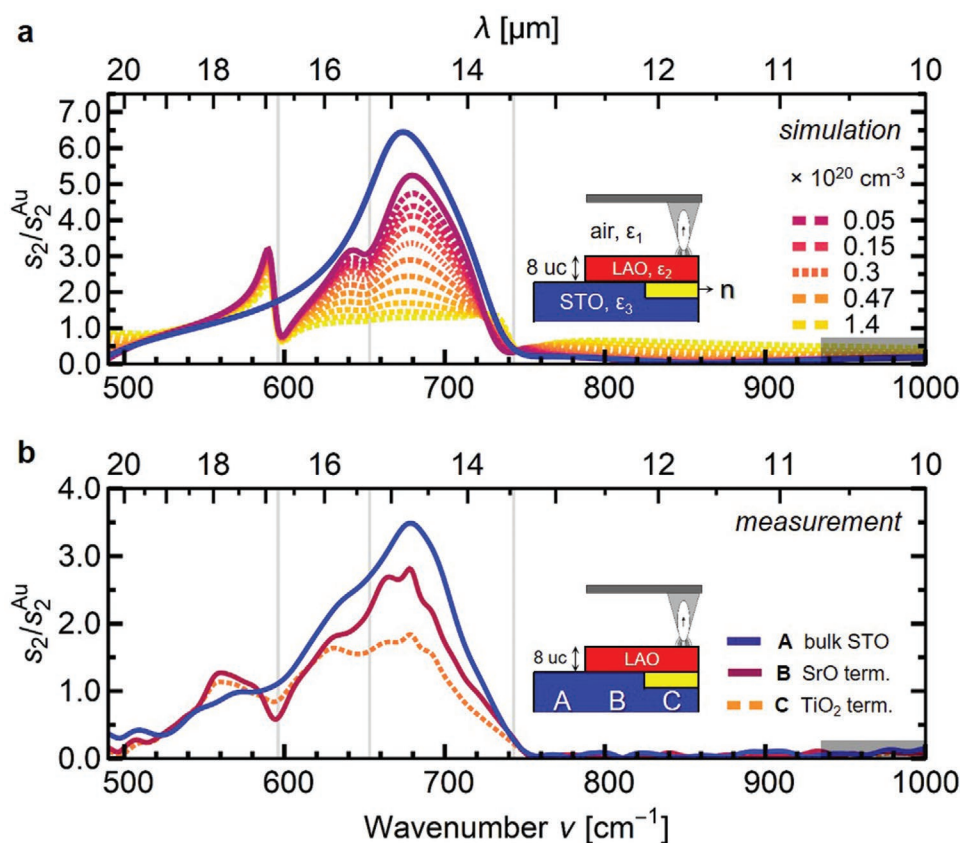


Figure 4. Influence of free electrons at the interface. a) Simulation of near-field contrast spectra of the layered system with 2DEG (cf. Figure 3a), by introducing an additional layer of free electrons (yellow) based on a Drude model. Vertical grey lines are indicating the zero-crossings of ϵ_{LAO} (cf. Figure 2b) for comparison. b) Measurements of Au-normalized scattering amplitude (demodulation order $n = 2$) of LAO/STO samples with SrO termination (without 2DEG, violet solid line) and TiO_2 termination (with 2DEG, orange dashed line), respectively, showing the influence of free electrons at the interface on peak damping. The shadowed rectangles in (a, b) illustrate spectral overlap with previous publications.

amplitude fits the value (relative to STO) expected from initial simulations for 8 uc LAO very well (cf. Figure 4a, violet solid line). Adding 2DEG electrons to the interface (TiO_2 termination) yields the dashed orange curve, which exhibits strong damping of the main phonon peak at 680 cm^{-1} , as would be expected from the presence of free electrons at the interface (cf. Figure 4a, dashed lines). This showcases the predictive power of the utilized theoretical model, irrespective of the simplifications still present in its implementation, and allows for the quantitative extraction of electronic properties from measurements. The best agreement can be found for an electron density of approximately $3 \times 10^{19} \text{ cm}^{-3}$ (central dashed curve in Figure 4a), which corresponds to a total sheet electron density of $3 \times 10^{13} \text{ cm}^{-2}$ distributed homogeneously across a layer of 10 nm thickness, which is a realistic size according to theoretical and experimental results.^[20,36,37] This coincides well with the sheet carrier density of $4.34 \times 10^{13} \text{ cm}^{-2}$ obtained in Hall transport measurements.

Finally, we want to discuss our results and comment on the reproducibility of the spectral features and experimentally observed differences. It is known that experimental conditions in SNOM—such as tapping amplitude and tip shape—can influence the spectral response in both experiments and simulations.^[35] The general reproducibility of all our measurements

was proven by measuring at three different positions across the sample (see Supporting Information). The influence of charge carriers and LAO thickness are found to be significantly larger than the measurement uncertainty within one sample. Under these circumstances, spectra of different samples can be compared to each other, for example, by using the bulk STO near-field spectrum as a frame of reference, in which the quantitative influence of LAO layers and 2DEG properties becomes visible. The difference in normalized peak height was already mentioned in the context of Figure 3 and could arise from the geometrical parameters of the FDM used in these simulations. While we will investigate this influence in more detail, we are confident that a comparison between experiment and simulation is possible when taking this scaling factor into account. However, there are still differences between measurement and simulation—such as the damped and shifted LAO feature below 600 cm^{-1} in Figure 4b—that cannot be explained by scaling or the presence of free charge carriers. Looking to the near future, we are going beyond the treatment of materials as homogeneous media described by bulk dielectric functions and will implement additional influences such as strain, confinement, anisotropy, and nonhomogeneous electron distributions. As these effects are ubiquitous on the nanoscale,

their implementation will have a great impact on the whole materials science community.

Investigating a variety of samples with carefully engineered differences in electron density, mobility, and LAO lattice defects will benchmark our models and improve their predictive accuracy. This goes hand in hand with extensive parameter variation studies on electron density n , mobility μ , effective mass m^* , and 2DEG thickness d_{2DEG} , to judge the impact of approximations and averaging in each of these parameters.

Beyond that, the spectroscopic investigation could be broadened by combining the near-field response in the phonon region—as presented here—with a future search for the plasmon near-field resonance. This could lead to a better separation of the damping influences of lattice defects and electrons. Furthermore, testing our model with temperature-dependent measurements in a cryo-SNOM setup^[15] will improve the disentanglement of electron density and mobility, as the latter dramatically increases at low temperatures.^[7]

3. Conclusion

SNOM enables the non-destructive subsurface investigation of interface effects in planar thin-film geometries, for example, in heterostructures of complex transition metal oxides or van-der-Waals heterostructures of 2D materials.^[39] In principle, different layers or interfaces can be addressed by probing at the different spectral regions of the relevant physical excitations (phonon and free charge carrier oscillations). However, the non-trivial SNOM response resulting from tip-sample coupling makes detailed comparison to proper theoretical descriptions necessary.

In this work, a broadband near-field spectroscopic investigation of LAO/STO phonons revealed distinct spectral features that contain both information about the thickness and lattice properties of the LAO top layer and information about free charge carriers at the interface: on the one hand, we were able to detect and characterize ultra-thin LAO layers with thicknesses of 4–16 unit cells (1.5–6 nm), demonstrating the impressive surface sensitivity of SNOM. On the other hand, by comparing different STO surface terminations, we could unambiguously show that the presence of the 2DEG at the LAO/STO interface leads to a reduction of the scattering amplitude of the LAO/STO phonon peak. We found the best spectral match for a charge carrier density of $3 \times 10^{13} \text{ cm}^{-2}$ which is in good agreement with the value of $4.34 \times 10^{13} \text{ cm}^{-2}$ obtained in Hall measurements averaged over large areas. Our spectroscopic investigation of these key parameters, the LAO layer thickness and the electron density, was enabled by an improved modeling of the SNOM response with the combination of Finite Dipole Model and Transfer Matrix Method.

Using these results, SNOM imaging at distinctly chosen frequencies can be performed in the future to learn about the 2DEG formation processes and identify influences of local defect structures such as oxygen vacancies or surface modifications.^[5,10] Additional experimental and theoretical refinement will allow for the investigation of nonlocal effects, plasmon-phonon coupling in the electrons damping factor or the vertical distribution of the LAO/STO 2DEG. Even now, our modeling

enables the prediction of effects like an increased carrier mobility on the spectral response of LAO/STO, which can be addressed in the future via cryo-SNOM^[15] at low temperatures. Our work sets the basis for spectroscopic SNOM investigations of ultra-thin heterostructures, which is applicable to a variety of buried oxide heterointerfaces and van-der-Waals heterostructures and will enable deeper insight into charge-transfer phenomena and linked properties, which are hard to access with other methods.

4. Experimental Section

A detailed description of the sample fabrication, measurement conditions, data analysis, and theoretical modeling is presented in the Supporting Information (SI).

Sample Preparation: All samples were grown on pre-annealed, TiO₂-terminated STO (100) single crystals, achieved via wet-chemical HF treatment. LAO thin films were deposited using pulsed laser deposition (PLD) and SrO termination was achieved by deposition of a single unit cell of SrO on a TiO₂-terminated STO (100) single crystal using the same PLD. High-pressure reflection high-energy electron diffraction (RHEED) was used to monitor the growth process. Clear intensity oscillations of the specular spot were visible for all samples, indicating a layer-by-layer growth mode. Further details can be found in the SI.

Measurements: Nano-FTIR measurements were done using a commercial s-SNOM (Neaspec GmbH) in a nano-FTIR setup with synchrotron illumination from the Metrology Light Source (MLS) at Physikalisch-Technische Bundesanstalt (PTB) Berlin.^[16] The storage ring was operated in a mode characterized by a low horizontal emittance, therefore leading to both a low beam size and a low beam divergence, making this mode particularly suited for s-SNOM measurements.^[40] All signals were demodulated at a higher harmonic of the tip oscillation ($n\Omega_{\text{tip}}$, $n = 2$) and normalized to thermally evaporated gold of 100 nm thickness in close vicinity to measurement locations and the resulting spectra were compared for three different locations on each sample to exclude outliers.

Theoretical Modeling: To model s-SNOM contrast, the finite dipole model^[28] was employed in combination with a transfer matrix method, resulting in a powerful predictive tool to simulate the near-field response of arbitrarily layered systems with known dielectric function^[17] (Figure 2a). Bulk dielectric functions of STO and LAO in the spectral region of interest were calculated from far-field measurements of the phonon resonances,^[31,32] fitted using the Berreman-Unterwald-Lowndes factorized form.^[30,41]

To include the influence of 2DEG free charge carriers on the dielectric function, a term following the Drude model was added for an interface layer of 10 nm thickness, consistent with Density Functional Theory and Poisson–Schrödinger simulations,^[20,36] and using an averaged effective mass of $m^* = 3.2 m_0$ as predicted by First Principles calculations^[42] and measured experimentally.^[37] Real values for average sheet carrier densities and electron mobilities of all samples were determined by Hall measurements.

Supporting Information

Supporting Information is available from the Wiley Online Library or from the author.

Acknowledgements

This work was supported by the German Research Foundation (DFG) under Grant Agreement no. TA 848/7-1. B.K. and G.U. acknowledge

funding from the EMPIR programme (JRP ADVENT) co-financed by the Participating States and from the European Union's Horizon 2020 research and innovation programme. M.R and F.G. acknowledge financial support from German Research Foundation DFG FG 1604 (No. 315025796).

Open access funding enabled and organized by Projekt DEAL.

Conflict of Interest

The authors declare no conflict of interest.

Keywords

2D electron systems, electronic properties, $\text{LaAlO}_3/\text{SrTiO}_3$, near-field spectroscopy, oxide heterostructures

Received: June 4, 2020

Revised: July 16, 2020

Published online:

- [1] M. Imada, A. Fujimori, Y. Tokura, *Rev. Mod. Phys.* **1998**, *70*, 1039.
- [2] a) R. Moos, K. H. Hardtl, *J. Am. Ceram. Soc.* **1997**, *80*, 2549; b) T. L. Meyer, A. Herklotz, V. Lauter, J. W. Freeland, J. Nichols, E.-J. Guo, S. Lee, T. Z. Ward, N. Balke, S. V. Kalinin, M. R. Fitzsimmons, H. N. Lee, *Phys. Rev. B* **2016**, *94*, 174432.
- [3] M. Lewin, C. Baeumer, F. Gunkel, A. Schwedt, F. Gaussmann, J. Wueppen, P. Meuffels, B. Jungbluth, J. Mayer, R. Dittmann, R. Waser, T. Taubner, *Adv. Funct. Mater.* **2018**, *28*, 1802834.
- [4] a) A. Brinkman, M. Huijben, M. van Zalk, J. Huijben, U. Zeitler, J. C. Maan, W. G. van der Wiel, G. Rijnders, D. H. A. Blank, H. Hilgenkamp, *Nat. Mater.* **2007**, *6*, 493; b) J.-S. Lee, Y. W. Xie, H. K. Sato, C. Bell, Y. Hikita, H. Y. Hwang, C.-C. Kao, *Nat. Mater.* **2013**, *12*, 703; c) L. Li, C. Richter, J. Mannhart, R. C. Ashoori, *Nat. Phys.* **2011**, *7*, 762.
- [5] F. Gunkel, C. Bell, H. Inoue, B. Kim, A. G. Swartz, T. A. Merz, Y. Hikita, S. Harashima, H. K. Sato, M. Minohara, S. Hoffmann-Eifert, R. Dittmann, H. Y. Hwang, *Phys. Rev. X* **2016**, *6*, 031035.
- [6] H. Y. Hwang, Y. Iwasa, M. Kawasaki, B. Keimer, N. Nagaosa, Y. Tokura, *Nat. Mater.* **2012**, *11*, 103.
- [7] A. Ohtomo, H. Y. Hwang, *Nature* **2004**, *427*, 423.
- [8] J. Mannhart, D. H. A. Blank, H. Y. Hwang, A. J. Millis, J.-M. Triscone, *MRS Bull.* **2008**, *33*, 1027.
- [9] S. Gariglio, M. Gabay, J.-M. Triscone, *APL Mater.* **2016**, *4*, 060701.
- [10] F. Gunkel, S. Wicklein, S. Hoffmann-Eifert, P. Meuffels, P. Brinks, M. Huijben, G. Rijnders, R. Waser, R. Dittmann, *Nanoscale* **2015**, *7*, 1013.
- [11] a) F. Gunkel, R. Waser, A. H. H. Ramadan, R. A. de Souza, S. Hoffmann-Eifert, R. Dittmann, *Phys. Rev. B* **2016**, *93*, 245431; b) F. Gunkel, R. A. Heinen, S. Hoffmann-Eifert, L. Jin, C.-L. Jia, R. Dittmann, *ACS Appl. Mater. Interfaces* **2017**, *9*, 10888.
- [12] A. Ohtomo, D. A. Muller, J. L. Grazul, H. Y. Hwang, *Nature* **2002**, *419*, 378.
- [13] a) F. Keilmann, R. Hillenbrand, *Philos. Trans. R. Soc., A* **2004**, *362*, 787; b) A. Huber, N. Ocelic, T. Taubner, R. Hillenbrand, *Nano Lett.* **2006**, *6*, 774.
- [14] L. Cheng, D.-L. Wang, S.-Y. Dai, Y.-D. Yan, X.-D. Fan, L.-M. Wei, C.-G. Zheng, *J. Infrared Millim. Waves* **2017**, *36*, 534.
- [15] W. Luo, M. Boselli, J.-M. Pournirol, I. Arizzone, J. Teyssier, D. van der Marel, S. Gariglio, J.-M. Triscone, A. B. Kuzmenko, *Nat. Commun.* **2019**, *10*, 2774.
- [16] P. Hermann, A. Hoehl, P. Patoka, F. Huth, E. Rühl, G. Ulm, *Opt. Express* **2013**, *21*, 2913.
- [17] B. Hauer, A. P. Engelhardt, T. Taubner, *Opt. Express* **2012**, *20*, 13173.
- [18] *Nat. Mater.* **2012**, *11*, 91.
- [19] F. Gunkel, P. Brinks, S. Hoffmann-Eifert, R. Dittmann, M. Huijben, J. E. Kleibuker, G. Koster, G. Rijnders, R. Waser, *Appl. Phys. Lett.* **2012**, *100*, 052103.
- [20] A. Janotti, L. Bjaalie, L. Gordon, C. G. van de Walle, *Phys. Rev. B* **2012**, *86*, 241108.
- [21] a) N. Nakagawa, H. Y. Hwang, D. A. Muller, *Nat. Mater.* **2006**, *5*, 204; b) L. Yu, A. Zunger, *Nat. Commun.* **2014**, *5*, 5118; c) H. Lee, N. Campbell, J. Lee, T. J. Asel, T. R. Paudel, H. Zhou, J. W. Lee, B. Noesges, J. Seo, B. Park, L. J. Brillson, S. H. Oh, E. Y. Tsymlal, M. S. Rzchowski, C. B. Eom, *Nat. Mater.* **2018**, *17*, 231.
- [22] T. Taubner, R. Hillenbrand, F. Keilmann, *J. Microsc.* **2003**, *210*, 311.
- [23] B. Knoll, F. Keilmann, *Nature* **1999**, *399*, 134.
- [24] F. Huth, A. Govyadinov, S. Amarie, W. Nuansing, F. Keilmann, R. Hillenbrand, *Nano Lett.* **2012**, *12*, 3973.
- [25] a) A. S. McLeod, E. van Heumen, J. G. Ramirez, S. Wang, T. Saerbeck, S. Guenon, M. Goldflam, L. Anderegg, P. Kelly, A. Mueller, M. K. Liu, I. K. Schuller, D. N. Basov, *Nat. Phys.* **2017**, *13*, 80; b) J. Döring, H.-G. von Ribbeck, M. Fehrenbacher, S. C. Kehr, L. M. Eng, *Appl. Phys. Lett.* **2014**, *105*, 053109; c) H. U. Yang, E. Hebestreit, E. E. Josberger, M. B. Raschke, *Rev. Sci. Instrum.* **2013**, *84*, 023701.
- [26] R. Hillenbrand, T. Taubner, F. Keilmann, *Nature* **2002**, *418*, 159.
- [27] F. Mooshammer, F. Sandner, M. A. Huber, M. Zizlsperger, H. Weigand, M. Plankl, C. Weyrich, M. Lanius, J. Kampmeier, G. Mussler, D. Grützmacher, J. L. Boland, T. L. Cocker, R. Huber, *Nano Lett.* **2018**, *18*, 7515.
- [28] A. Cvitkovic, N. Ocelic, R. Hillenbrand, *Opt. Express* **2007**, *15*, 8550.
- [29] L. Jung, J. Pries, T. W. W. Maß, M. Lewin, D. S. Boyuk, A. T. Mohabir, M. A. Filler, M. Wuttig, T. Taubner, *ACS Photonics* **2019**, *6*, 1744.
- [30] S. Schöche, T. Hofmann, D. Nilsson, A. Kakanakova-Georgieva, E. Janzén, P. Kühne, K. Lorenz, M. Schubert, V. Darakchieva, *J. Appl. Phys.* **2017**, *121*, 205701.
- [31] K. Kamarás, K.-L. Barth, F. Keilmann, R. Henn, M. Reedyk, C. Thomsen, M. Cardona, J. Kircher, P. L. Richards, J.-L. Stehlé, *J. Appl. Phys.* **1995**, *78*, 1235.
- [32] T. Willett-Gies, E. DeLong, S. Zollner, *Thin Solid Films* **2014**, *571*, 620.
- [33] a) E. Yoxall, *Ph.D. Thesis*, Imperial College (London), **2013**; b) P. G. Gucciardi, G. Bachelier, M. Allegrini, *J. Appl. Phys.* **2006**, *99*, 124309; c) N. Ocelic, *Ph.D. Thesis*, TU (München), **2007**.
- [34] K. L. Kostov, F. O. Schumann, S. Polzin, D. Sander, W. Widdra, *Phys. Rev. B* **2016**, *94*, 075438.
- [35] P. McArdle, D. J. Lahneman, A. Biswas, F. Keilmann, M. M. Qazilbash, *Phys. Rev. Res.* **2020**, *2*, 023272.
- [36] D. Li, S. Lemal, S. Gariglio, Z. Wu, A. Fête, M. Boselli, P. Ghosez, J.-M. Triscone, *Adv. Sci.* **2018**, *5*, 1800242.
- [37] A. Dubroka, M. Rössle, K. W. Kim, V. K. Malik, L. Schultz, S. Thiel, C. W. Schneider, J. Mannhart, G. Herranz, O. Copie, M. Bibes, A. Barthélémy, C. Bernhard, *Phys. Rev. Lett.* **2010**, *104*, 156807.
- [38] F. Gervais, J.-L. Servoin, A. Baratoiff, J. G. Bednorz, G. Binnig, *Phys. Rev. B* **1993**, *47*, 8187.
- [39] a) D. N. Basov, M. M. Fogler, F. J. García de Abajo, *Science* **2016**, *354*, aag1992; b) T. Low, A. Chaves, J. D. Caldwell, A. Kumar, N. X. Fang, P. Avouris, T. F. Heinz, F. Guinea, L. Martin-Moreno, F. Koppens, *Nat. Mater.* **2017**, *16*, 182.
- [40] P. Hermann, B. Kästner, A. Hoehl, V. Kashcheyevs, P. Patoka, G. Ulrich, J. Feikes, M. Ries, T. Tydecks, B. Beckhoff, E. Rühl, G. Ulm, *Opt. Express* **2017**, *25*, 16574.
- [41] a) D. W. Berreman, F. C. Unterwald, *Phys. Rev.* **1968**, *174*, 791; b) R. P. Lowndes, *Phys. Rev. B* **1970**, *1*, 2754.
- [42] P. Delugas, A. Filippetti, V. Fiorentini, D. I. Bilc, D. Fontaine, P. Ghosez, *Phys. Rev. Lett.* **2011**, *106*, 166807.